OXFORD Regenerative Biomaterials

Regenerative Biomaterials, 2024, **11**, rbae083
https://doi.org/10.1093/rb/rbae083
Advance Access Publication Date: 25 July 2024
Research article

A bilayer bioengineered patch with sequential dual-growth factor release to promote vascularization in bladder reconstruction

Jian Zhao[1,2,3,‡], Haoqian Zhang[4,‡], Zhengyun Ling[2,5,‡], Ziyan An[1,2], Shuwei Xiao[6], Pengchao Wang[2], Zhouyang Fu[2], Jinpeng Shao[1,2], Yanfeng Sun[7,*] and Weijun Fu[2,*]

[1]Medical School of PLA, Beijing 100853, China
[2]Department of Urology, The Third Medical Center, PLA General Hospital, Beijing 100039, China
[3]Department of Urology, 960th Hospital of PLA, Jinan 250031, China
[4]Inner Mongolia Medical University, Hohhot, Inner Mongolia 010050, China
[5]School of Medicine, Nankai University, Tianjin 300071, China
[6]Department of Urology, Air Force Medical Center, Beijing 100142, China
[7]Department of Pediatrics, The Third Medical Center, PLA General Hospital, Beijing 100039, China

*Correspondence address. E-mail: eksyf@qq.com (Y. S.); fuweijun@hotmail.com (W. F.)

‡These authors contributed equally to this work.

Abstract

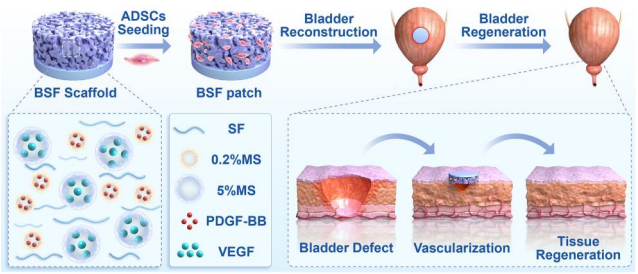

Bladder tissue engineering holds promise for addressing bladder defects resulting from congenital or acquired bladder diseases. However, inadequate vascularization significantly impacts the survival and function of engineered tissues after transplantation. Herein, a novel bilayer silk fibroin (BSF) scaffold was fabricated with the capability of vascular endothelial growth factor (VEGF) and platelet derived growth factor-BB (PDGF-BB) sequential release. The outer layer of the scaffold was composed of compact SF film with waterproofness to mimic the serosa of the bladder. The inner layer was constructed of porous SF matrix incorporated with SF microspheres (MS) loaded with VEGF and PDGF-BB. We found that the 5% (w/v) MS-incorporated scaffold exhibited a rapid release of VEGF, whereas the 0.2% (w/v) MS-incorporated scaffold demonstrated a slow and sustained release of PDGF-BB. The BSF scaffold exhibited good biocompatibility and promoted endothelial cell migration, tube formation and enhanced endothelial differentiation of adipose derived stem cells (ADSCs) *in vitro*. The BSF patch was constructed by seeding ADSCs on the BSF scaffold. After *in vivo* transplantation, not only could the BSF patch facilitate the regeneration of urothelium and smooth muscle, but more importantly, stimulate the regeneration of blood vessels. This study demonstrated that the BSF patch exhibited excellent vascularization capability in bladder reconstruction and offered a viable functional bioengineered patch for future clinical studies.

Keywords: bladder tissue engineering; microsphere; sequential release; vascularization

Introduction

Bladder defects, whether anatomical or functional, impair urinary storage and voiding functions, resulting in reduced quality of life [1]. Conventional enterocystoplasty is often accompanied by a series of complications, such as infection, stone formation, metabolic disorder and malignancy, due to the substantial structural and functional disparity between the intestine and the bladder [2–6]. Consequently, an innovative approach to bladder reconstruction is urgently required. In recent years, with the development of biomaterials and stem cells, tissue engineering has been a promising strategy for bladder repairment and reconstruction [7–11]. Scaffold material is an important part of bladder tissue engineering. Both naturally derived material represented by bladder acellular matrix and synthetic polymer represented by polyurethanes have been used in bladder tissue engineering [12, 13]. Silk fibroin, derived from *Bombyx mori* cocoons, has good plasticity and can be used to fabricate thin films, sponges, hydrogels and microspheres [14]. Moreover, silk fibroin owns good biocompatibility and controllable mechanical properties, making it very suitable for the repair and reconstruction of the bladder [15].

The bladder is a multi-layered organ with smooth muscle as its main structure. Adequate blood supply is necessary to maintain its normal function. However, studies reveal that the maximum distance between capillaries in the body is 200 μm, imposing a constraint on oxygen diffusion in tissues [16]. Therefore, ineffective vascularization will lead to graft atrophy and

Received: February 4, 2024. **Revised:** June 15, 2024. **Accepted:** June 25, 2024

necrosis [17]. Thus, vascularization is a major problem that affects the clinical translation of bladder tissue engineering. There are few researches on vascularization in bladder tissue engineering. Scaffold prevascularization with omentum embedding seems to be a promising approach, but it is time-consuming and can cause secondary damage to the host [18]. Therefore, it is necessary to explore a simple and minimally invasive method to promote vascularization in bladder tissue engineering.

Besides prevascularization, the promotion of host vascular infiltration [19–24] is another strategy for vascularization, among which surface modification on tissue-engineered scaffolds with angiogenic growth factors seems to be a potential method [19, 25]. There are many kinds of angiogenic growth factors, including vascular endothelial growth factor (VEGF), platelet derived growth factor (PDGF), fibroblast growth factor (FGF), angiopoietin (ANG), etc. Specifically, VEGF can induce the migration and branching of vascular endothelial cells during the initiation stage of vascularization process, which plays an important role in promoting the germination of capillaries [26]. Meanwhile, PDGF can stimulate the recruitment and proliferation of smooth muscle cells and fibroblasts around endothelial cells during the maturation stage of vascularization process, which is the key to promoting capillary maturation [27]. However, a single growth factor may not effectively enhance vascularization. Researches in drug delivery indicate that the sequential release of growth factors which mimic their temporal release and spatial distribution *in vivo* can play a synergistic role in promoting vascularization [28].

Microspheres refer to spherical particles with a diameter <1000 μm. The high specific surface area of microspheres renders them excellent carriers for drug delivery [29]. More importantly, the drug release property can be tuned by changing the particle size and surface morphology of the microspheres, which makes microspheres ideal carriers for achieving sequential release of growth factors [30].

Adipose derived stem cells (ADSCs), known for their extensive sources, convenient isolation and multi-lineage differentiation potential, are commonly used in bladder tissue engineering [31]. ADSCs not only regulate cell migration and microenvironment through paracrine signaling [32], but also can differentiate into smooth muscle cells or endothelial cells under specific conditions, facilitating vascularization and tissue regeneration [33, 34]. Furthermore, studies have demonstrated that bladder scaffolds seeded with ADSCs show better effect of tissue repairment than the non-seeded ones [35].

In this study, we attempted to fabricate a bilayer bioengineered patch with sequential dual-growth factor release to promote vascularization in bladder reconstruction. The bilayer silk fibroin (BSF) scaffold was made by silk fibroin because of its excellent biocompatibility. The outer layer of the BSF scaffold was composed of SF film with toughness and waterproofness to mimic the serosa of the bladder, which provided mechanical support and prevented urine leakage. The inner layer of the BSF scaffold was composed of porous SF matrix incorporated with tunable growth factor-loaded SF microspheres, which could achieve the sequential release of VEGF and PDGF-BB. After seeding ADSCs on the BSF scaffold, the BSF patch was constructed. To determine the suitable concentrations for microspheres preparation, the release profiles of growth factors were assessed. Subsequently, *in vitro* experiments were used to examine the biocompatibility and angiogenic ability of the BSF scaffold. Finally, a rat bladder defect model was employed to evaluate the impact of the BSF patch on vascularization and regeneration of the reconstructed bladder *in vivo*.

Materials and methods

Preparation of SF microspheres

SF microspheres were prepared as previously reported [14]. In brief, SF and polyvinyl alcohol (PVA, Sigma, Germany) solution were mixed at the same concentration (0.2%, 1% and 5%) in a ratio of 1:4 (v/v). The growth factor-loaded microspheres were fabricated by adding 200 ng/ml VEGF (Peprotech, USA) or PDGF-BB (Peprotech, USA) to the SF solution before mixing with PVA solution. The mixed solution was sonicated with an ultrasonic processer (950E, SCIENTZ, China) at 25% amplitude for 30 s. The mixture was poured into a petri dish evenly and was dried overnight in fume hood. The dried film was dissolved in ultrapure water under shaking for 30 min and centrifuged twice at 11 000 rpm at 4 °C for 20 min. The SF microspheres were obtained by resuspending the precipitate in ultrapure water. The microspheres fabricated from 0.2%, 1% or 5% SF/PVA concentration were termed as 0.2% MS, 1% MS or 5% MS, respectively.

Preparation of BSF scaffold

BSF scaffold was prepared according to the method described by Zhang with partial modifications [36]. The SF film was obtained by adding 10% SF solution into a petri dish and dried at 60 °C for 4 h. Then, 6% SF solution was mixed with SF microsphere suspension in a ratio of 1:3 (v/v). The mixture was poured onto the film, frozen at −80 °C overnight and lyophilized for 24 h in a freeze-drying machine (10 N, SCIENTZ, China) to obtain the BSF scaffold. Then the scaffold was treated with 90% methanol (SCR, China) for 1 h to induce crosslinking. After re-lyophilization, the BSF scaffold was cut into a cylinder with a diameter of 8 mm and a height of 1.5 mm. The BSF scaffold without microsphere incorporation was termed as BSF, and the BSF scaffold incorporated with 0.2% MS, 1% MS or 5% MS was termed as BSF-0.2% MS, BSF-1% MS or BSF-5% MS, respectively. The unloaded, VEGF-loaded, PDGF-BB-loaded or VEGF/PDGF-BB-loaded BSF scaffold was termed as BSF-MS, BSF-MS-VEGF, BSF-MS-PDGF or BSF-MS-V/P, respectively.

Scanning electron microscope imaging

SF microsphere (0.2%, 1% and 5%) suspension was diluted 50 times, dripped onto the silicon wafer and dried overnight to prepare the sample. BSF scaffold was lyophilized and cut along the transverse axis to prepare the sample. After being coated with gold, the samples were observed by a scanning electron microscope (SEM; SU8220, HITACHI, Japan) to evaluate the surface structure. The images of SF microspheres were processed using Image J (NIH, USA), and the particle size distribution was analyzed using Origin 2021 software.

Loading and release of growth factors

The loading efficiency of growth factors was measured by collecting the supernatant obtained during the preparation of SF microspheres using VEGF ELISA Kit (Abcam, UK) and PDGF-BB ELISA Kit (Abcam, UK). The BSF scaffold loaded with growth factors was incubated in PBS at 37 °C with shaking. The supernatant was collected for ELISA analysis on day 1, 3, 7, 14, 21 and 28. The cumulative release of growth factors was analyzed by GraphPad Prism 8.0.2 software.

Mechanical property of BSF scaffold

BSF scaffold was prepared into a cube of 40 mm × 20 mm × 3 mm. The mean break stress was obtained by using a universal

mechanical testing machine (68SC-1, Instron, USA) at a constant speed of 2 mm/s until the scaffold was broken.

In vitro degradation of BSF scaffold

BSF scaffold was cut into a cylinder with a diameter of 8 mm and a height of 1.5 mm. The dry weight of the scaffold was recorded as M0. Subsequently, the scaffold was incubated in simulated body fluids at 37 °C with shaking. On day 7, 14, 21 and 28, the scaffold was dried and weighed as M1. Weight loss (%) = (M0 − M1)/M0 × 100%.

Isolation, culture and characterization of ADSCs

ADSCs were isolated as previously reported [18]. In brief, inguinal adipose tissues from 2 weeks old Sprague Dawley (SD) rats were harvested and rinsed with PBS three times. Then the adipose tissues were cut into small pieces and digested with 0.25% trypsin at 37 °C for 30 min. After digestion, the supernatant was filtered and centrifuged at 1200 rpm for 10 min. Finally, the precipitate was resuspended in Dulbecco's modified eagle medium (DMEM) supplemented with 10% fetal bovine serum (FBS) and cultured in an incubator at 37 °C and 5% CO_2. The culture medium was changed every 2 days. The third passage of ADSCs was identified by flow cytometry with a panel of antibodies, including CD29, CD45, CD90, CD106 and CD31. The third to fifth passages of ADSCs were used for subsequent experiments.

Effect of BSF scaffold on cell viability and proliferation

ADSCs were seeded on sterilized BSF scaffold with a cell density of 1×10^6 cells/ml. The BSF patch was cultured in DMEM at 37 °C and 5% CO_2 with the culture medium being replaced every 2 days. The cell viability was assessed using a fluorescent live/dead activity assay kit (KeyGEN Biotech, China) on day 1 and 7 according to the protocol. The BSF patch was visualized under a confocal laser scanning microscope (LSM900, ZEISS, Germany). At the same time, the cell proliferation was analyzed using a Cell Counting Kit-8 (CCK-8, Dojindo, Japan) on day 1, 3, 5 and 7 according to the protocol. The absorbance at 450 nm was measured by a microplate reader (Molecular Versa max, USA). ADSCs cultured in the petri dish were served as the control group.

HUVEC migration and tube formation

HUVECs (CTCC, China) were cultured in endothelial cell culture medium (ECM, China) supplemented with 10% FBS. The culture medium was replaced every 2 days and the third to sixth passages of HUVECs were used in the experiments. The BSF scaffold was immersed in serum-free ECM at 37 °C for 72 h and the extract was collected. HUVECs were stained with PKH26 (Solarbio, China) before being seeded in 6-well plate. A scratch was performed in the center of the well using a 200 μl tip, then 2 ml extract was added into each well. Pictures were captured at 0 and 24 h using a fluorescence microscope (Ti2, NIKON ECLIPSE, Japan). The migration area was quantified using Image J.

The BSF scaffold was immersed in ECM containing 10% FBS at 37 °C for 72 h and the extract was collected. A 24-well plate was placed on ice, and 150 μl growth factor-reduced Matrigel (Corning, USA) was coated on each well. After incubating at 37 °C for 30 min, 1×10^5 HUVECs in 500 μL extract were seeded in each well and cultured at 37 °C and 5% CO_2. Photos of capillary-like tubes were captured by an optical microscope (Ts2, NIKON ECLIPSE, Japan) 4 h after seeding. The number of tubes and the length of tubes were quantified using Image J.

Q-PCR analysis

The third passage of ADSCs were seeded on the BSF scaffold in a 24-well plate at the density of 1×10^7 cells/ml. They were cultured in ECM for 21 days *in vitro*. The culture medium was changed every 2 days. The differentiated ADSCs were collected on day 7, 14 and 21, the total RNA was extracted using Trizol reagent (Invitrogen, USA). Meanwhile, the total RNA of HUVECs was extracted as the positive control. RNA was reverse transcribed to cDNA by a commercially available PrimeScript RT Reagent Kit (Takara, Japan). The gene expression levels of PECAM-1 and KDR were analyzed by quantitative PCR using a LightCycler 96 system (Roche, Switzerland) with a SYBR Primix kit (Takara, Japan). The primer sequence is listed in Supplementary Table S1.

Immunofluorescence staining

After 14 days of differentiation, the BSF patch was rinsed with PBS, fixed with 4% paraformaldehyde (Beyotime, China) for 1 h and then subjected to frozen section. The sections were permeabilized with 0.1% Triton-X100 (Beyotime, China) for 30 min, blocked with protein block (Abcam, UK) for 30 min, and then incubated with anti-CD31 antibody (1:100, Abcam, UK) and anti-vWF antibody (1:100, Abcam, UK) overnight at 4 °C. After washed with PBS for three times, the sections were incubated with secondary antibody (1:250, Abcam, UK) and the nuclei were stained with DAPI. The sections were observed under a confocal laser scanning microscope (LSM900, ZEISS, Germany).

Acetylated-low-density lipoprotein/Ulex europaeus-1 (Ac-LDL/UEA-1) uptake

Ac-LDL/UEA-1 uptake was detected by incubating ADSCs differentiated for 14 days with 50 μg/ml of Ac-LDL labeled with Dil (Solarbio, China) for 4 h at 37 °C. After being washed twice with PBS, they were fixed in 4% paraformaldehyde for 15 min. Then they were incubated with 20 μg/ml of FITC-conjugated UEA-1 (Sigma Aldrich, USA) for 1 h at 37 °C. HUVECs were used as the positive control. The cells were visualized by a fluorescence microscope (Ti2, NIKON ECLIPSE, Japan).

Rat bladder reconstruction

Male SD rats of 8 weeks old were randomly divided into four groups: BSF-MS group, BSF-MS-VEGF group, BSF-MS-PDGF group and BSF-MS-V/P group. ADSCs were seeded on BSF scaffold in a 24-well plate with a cell density of 1×10^7 cells/ml, then the BSF patch was cultured in DMEM at 37 °C and 5% CO_2 for 3 days before operation. Animal experiments were approved by the Animal Experimental Ethics Committee of the People's Liberation Army General Hospital (Approval number: 2023-X19-29).

SD rats were anesthetized with pentobarbital (30 mg/kg) intraperitoneally and then shaved to expose the surgical site. A 2-cm longitudinal excision was made at the midline of the lower abdomen to expose the bladder. A 50% cystectomy was performed at the dome of the bladder, the whole layer of the bladder was removed and the BSF patch was used to repair the defect. The 5-0 nonabsorbable sutures were used to mark the repaired boundary at the four corners and 6-0 absorbable sutures were used to anastomose the remaining incision. The tightness of the suture was tested by injecting sterile saline into the repaired bladder *via* a 1 ml syringe. Finally, the lower abdominal incision was closed using 3-0 absorbable sutures.

Cystography

The SD rats were anesthetized with pentobarbital (30 mg/kg) intraperitoneally 4 weeks post-operation. The iopamidol (Aladdin, China) was diluted to a concentration of 30% (v/v) with sterile saline and then injected into the bladder using a 1 ml syringe until stress incontinence. X-ray films were obtained using a Quantum GX Micro-CT (PerkinElmer, USA).

Histological evaluation

Four weeks post-operation, samples of the bladder were harvested, fixed in 4% paraformaldehyde, dehydrated with graded ethanol, embedded in paraffin, sectioned into 5 μm slices and subjected to HE staining, Masson's trichrome staining and Immunofluorescence staining. HE and Masson trichrome staining were performed with standard protocols. Images were captured using an optical microscope (Ts2, NIKON ECLIPSE, Japan). Besides, sections were incubated with anti-pan cytokeratin antibody (AE1+AE3, 1:100, Abcam, UK), anti-alpha smooth muscle actin antibody (α-SMA, 1:100, Abcam, UK) and anti-CD31 antibody (1:100, Abcam, UK) at 4 °C overnight. After washed with PBS for three times, the sections were incubated with secondary antibody (1:250, Abcam, UK) and the nuclei were stained with DAPI. The sections were observed using a fluorescence microscope (Ti2, NIKON ECLIPSE, Japan).

Statistical analysis

Statistical analysis was performed using GraphPad Prism. All data were presented as mean ± standard deviation. The differences between groups were analyzed using two-tailed Student's t-test or one-way ANOVA test. $P < 0.05$ was considered as statistically significant. The data were indicated with * for $P < 0.05$, ** for $P < 0.01$, *** for $P < 0.001$, **** for $P < 0.0001$ and NS for no statistical significance.

Results and discussion

Preparation and characterization of SF microspheres

Microspheres prepared by different materials and methods exhibit diverse shapes, structures and functions [37–40]. Particle size, a pivotal parameter of microspheres, is affected by many factors such as the molecular weight of the ingredient, the concentration of the raw material and the synthesis method. Higher molecular weight and concentration of the raw material result in larger particle size of microspheres [41]. Nonetheless, increasing the ultrasonic amplitude during SF microsphere preparation leads to smaller particle sizes [14]. In our study, SF microspheres were fabricated by a simple phase separation method using SF and PVA solution at the same concentration. The SF microspheres fabricated from 0.2%, 1% and 5% SF/PVA concentration showed a spherical shape with smooth surface under SEM (Figure 1A–F). Their particle sizes ranged from about 100 nm to 7 μm, and the mean particle size was 0.32 ± 0.09 μm, 0.47 ± 0.15 μm, 4.37 ± 1.02 μm, respectively (Figure 1G–I). The particle size of 0.2% MS was similar to that of 1% MS, but the particle size of 5% MS was nearly 10 times larger than that of 0.2% MS, which may have great influence on the function of microspheres.

The drug loading and release profiles of microspheres are important parameters as well. Previous research indicates that loading and release profiles depend on factors such as hydrophilicity, surface charge, particle size, the molecular weight of drugs, as well as the binding method between microspheres and drugs [42]. A previous study on the loading profiles of SF microspheres reported that the encapsulation efficiency of E7, a small peptide for bone regeneration, was 22.6% because of its hydrophilicity. While the encapsulation efficiency of hydrophobic Rhodamine B was higher than 60% [36]. In our study, the SF microspheres were used for the encapsulation of VEGF and PDGF-BB. The

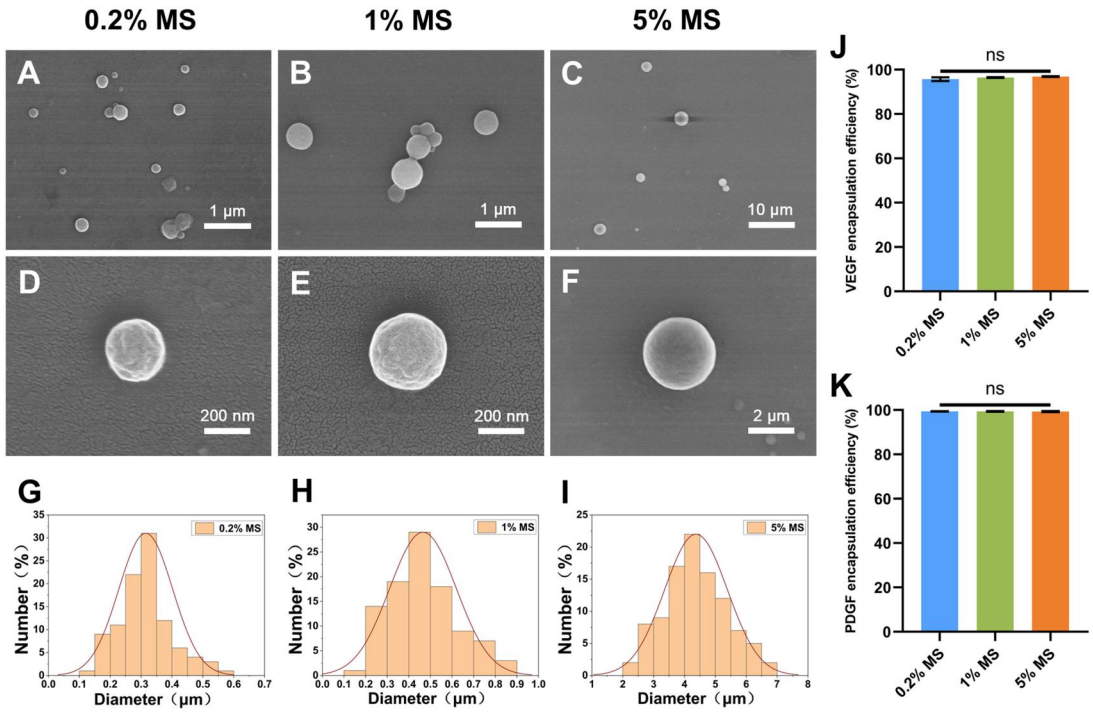

Figure 1. Preparation and characterization of SF microspheres. (**A**, **D**) SEM image of SF microspheres fabricated from 0.2% SF/PVA concentration. (**B**, **E**) SEM image of SF microspheres fabricated from 1% SF/PVA concentration. (**C**, **F**) SEM image of SF microspheres fabricated from 5% SF/PVA concentration. Particle size distribution of SF microspheres fabricated from 0.2% (**G**), 1% (**H**) and 5% (**I**) SF/PVA concentration. (**J**) Encapsulation efficiency of VEGF in SF microspheres. (**K**) Encapsulation efficiency of PDGF-BB in SF microspheres.

encapsulation efficiency of VEGF for the microspheres (0.2%, 1% and 5%) was 95.72 ± 0.80%, 96.45 ± 0.20% and 96.90 ± 0.16%, respectively (Figure 1J). The encapsulation efficiency of PDGF-BB for the microspheres (0.2%, 1% and 5%) was 99.35 ± 0.07%, 99.37 ± 0.13% and 99.29 ± 0.22% (Figure 1K), respectively, indicating the suitability of SF microspheres for loading these two growth factors.

Preparation and characterization of BSF scaffold

The bladder is a hollow organ with a multi-layered structure whose main function is to store and void urine through contraction and relaxation. Studies have demonstrated that scaffolds with bilayer structures and diverse functions significantly impact tissue repair [43–45]. Moreover, the bilayer design is also prevalent in the widely utilized 3D printing technique [46]. As shown in Figure 2A, the BSF scaffold was cut into a cylinder ($d = 8$ mm). SEM images demonstrated that the BSF scaffold showed an obvious double-layer structure. The outer layer was a smooth SF film with compact structure (Figure 2B), signified robust mechanical properties (Figure 2F) and waterproofness (Supplementary Figure S1), which had similar functions with serosa of the bladder wall. Conversely, the inner layer was a rough SF matrix with porous structure (Figure 2B), suggesting favorable cell adhesion capabilities, which had similar functions with submucosa and muscularis of the bladder wall. SF microspheres incorporated in the SF scaffold were demonstrated by SEM of the cross section (Figure 2C). The weight loss of BSF-0.2% MS, BSF-1% MS and BSF-5% MS on day 28 was 17.05 ± 1.59%, 17.32 ± 0.71% and 19.37 ± 2.45%, significantly higher than that of the BSF, which was 9.93 ± 2.29% (Figure 2G). While the weight loss was higher *in vivo* and the comparison was not that significant (Supplementary Figure S2).

Afterwards, we investigated the release profiles of VEGF and PDGF-BB from the BSF scaffold. Scaffold incorporated with different SF microspheres (0.2%, 1% and 5%) showed similar sustained release trend but at different rates (Figure 2D and E). The BSF-5% MS released VEGF and PDGF-BB more rapidly than the BSF-0.2% MS, potentially due to the aforementioned larger particle size. Particularly, the VEGF released by the BSF-5% MS was approximately six times more than the PDGF-BB released by the BSF-0.2% MS in the first 7 days, and both VEGF released by BSF-5% MS and PDGF-BB released by BSF-0.2% MS could last for more than 30 days, which was similar with the sequential release pattern of growth factors in the vascularization process. In order to mimic the sequential release of growth factors *in vivo*, 5% MS loaded with VEGF was employed to fabricate the BSF-MS-VEGF, 0.2% MS loaded with PDGF-BB was employed to fabricate the BSF-MS-PDGF and these two microspheres mixed together in a ratio of 1:1(w/w) were employed to fabricate the BSF-MS-V/P. These findings suggest that manipulating the particle size of SF microspheres enables sequential release of growth factors, offering extensive application potential. These results reveal that the bilayer structure of BSF scaffold is more in line with the bionic concept in tissue engineering. In addition, this bilayer scaffold provides a reproducible template for the construction of complex tissues and organs in tissue engineering.

Biocompatibility of BSF scaffold and its effect on HUVECs migration and tube formation

ADSCs were verified by the flow cytometry results that the isolated cells were positive for CD29 and CD90 but negative for CD45, CD106 and CD31 (Supplementary Figure S3). Meanwhile, the multi-lineage differentiation potential was demonstrated by the adipogenic, osteogenic and chondrogenic differentiation of ADSCs (Supplementary Figure S4). CCK-8 analysis showed that the cell proliferation rate

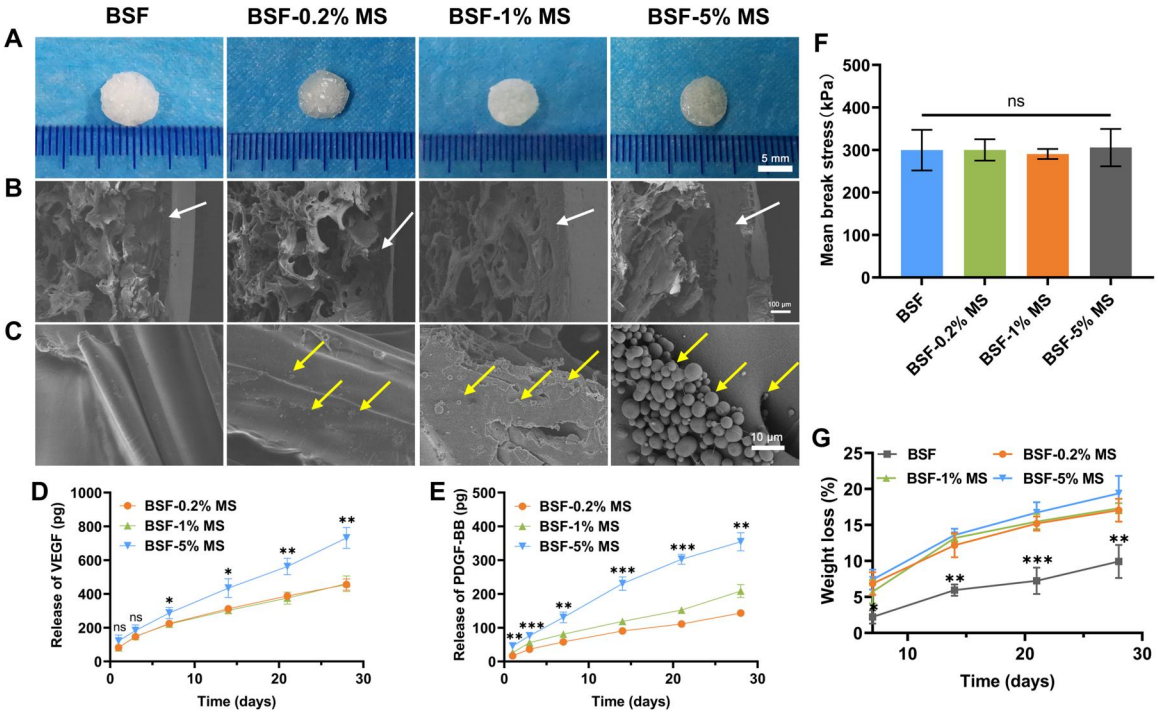

Figure 2. Preparation and characterization of BSF scaffold. (**A**) Gross images of BSF scaffold. (**B**) SEM images of BSF scaffold. The arrows indicate the SF film. (**C**) SEM images of the cross section of BSF scaffold. The arrows indicate the incorporated SF microspheres. (**D**) Cumulative release of VEGF from BSF scaffold ($n = 3$). (**E**) Cumulative release of PDGF-BB from BSF scaffold ($n = 3$). (**F**) Mean break stress of BSF scaffold ($n = 3$). (**G**) Weight loss (%) of BSF scaffold ($n = 3$).

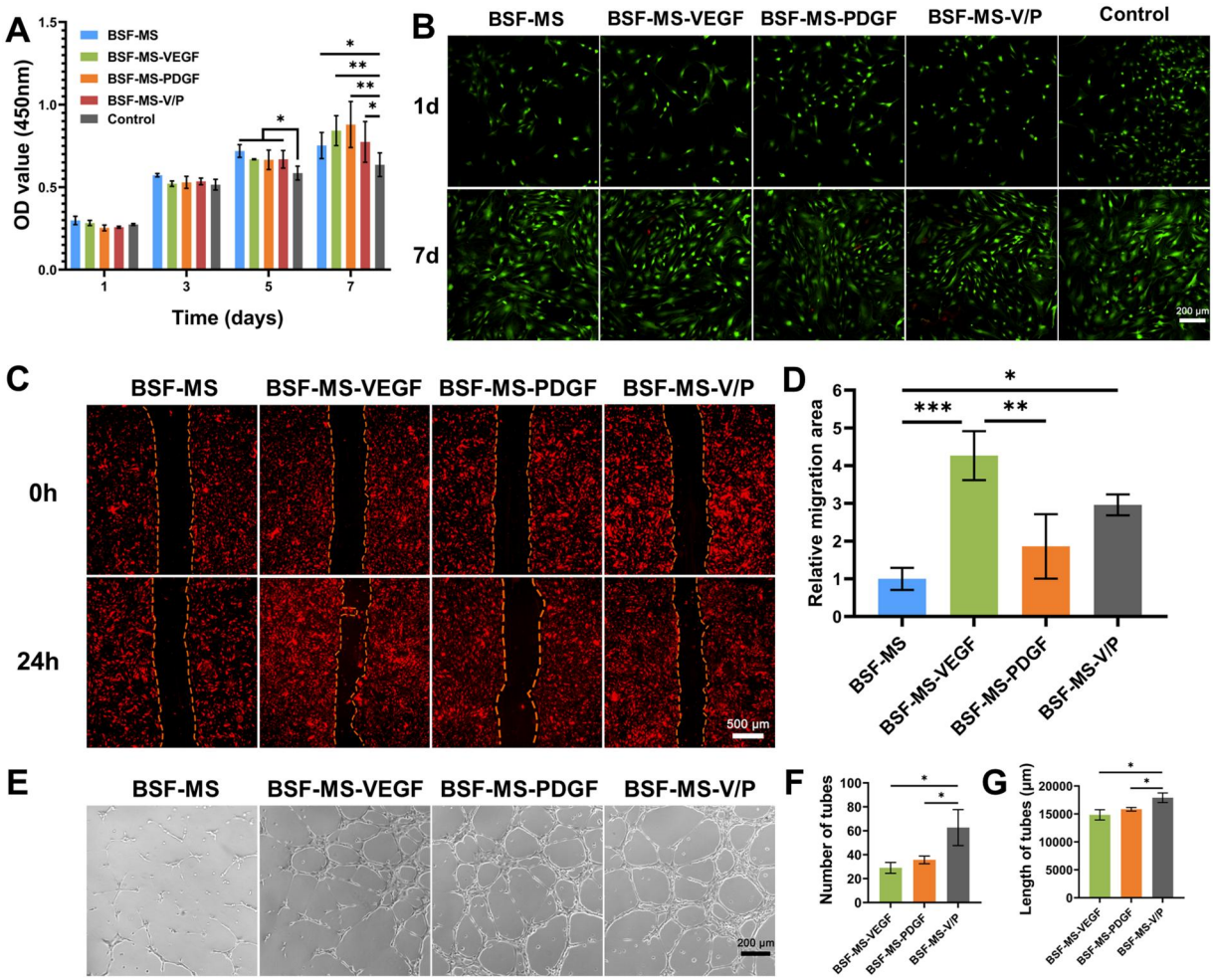

Figure 3. Biocompatibility of BSF scaffold and its effect on HUVECs migration and tube formation. (**A**) CCK-8 of ADSCs seeded on BSF scaffold on day 1, 3, 5 and 7 ($n = 3$). (**B**) Live/dead staining of ADSCs seeded on BSF scaffold on day 1 and 7. (**C**) Images of HUVECs migration at 0 and 24 h. The dotted lines indicate cell migration fronts. (**D**) Quantification of the relative migration area ($n = 3$). The migration area in the BSF-MS group was set as 1. (**E**) Images of HUVECs tube formation on Matrigel at 4 h. (**F**) Quantification of the number of tubes ($n = 3$). (**G**) Quantification of the length of tubes ($n = 3$).

increased over time and the OD values of ADSCs seeded on BSF scaffold were significantly higher than that of the control group on day 7 (Figure 3A). Live/dead staining also presented well proliferation of ADSCs from day 1 to day 7 in all groups with few dead cells observed, indicating good biocompatibility (Figure 3B).

Vascularization remains a crucial challenge in tissue engineering, significantly affecting the clinical translation of engineered tissues [47]. A small dose of growth factors can induce obvious biological effects, due to the high efficiency. Therefore, employing a scaffold loaded with angiogenic growth factors to recruit vascular endothelial cells emerges as a promising strategy to stimulate vascularization [48]. However, immature blood vessels triggered by VEGF alone are easy to leak out [49]. Hence, the sequential release of multiple angiogenic growth factors seems more reasonable to facilitate vascularization [50]. *In vitro* HUVECs scratch assay revealed that the BSF-MS-VEGF group had significantly larger relative migrating area than the BSF-MS group and the BSF-MS-PDGF group (Figure 3C and D). Also, the relative migrating area in the BSF-MS-V/P group was significantly larger than the BSF-MS group, suggesting that VEGF enhanced HUVECs migration.

Images of HUVECs tube formation showed fragmented tubes formed in the BSF-MS group compared with the other three groups (Figure 3E), indicating vascularization stimulation of VEGF and PDGF-BB. Further analysis by Image J demonstrated that the BSF-MS-V/P group had significantly better score on not only the number of tubes but also the length of tubes than the BSF-MS-VEGF group and the BSF-MS-PDGF group (Figure 3F and G), suggesting that sequential release of VEGF and PDGF-BB was prior in vascularization than VEGF or PDGF-BB alone. These findings underline that this combination of growth factors could recruit endothelial cells around the injured area and stimulate their assembly into tubular structures, paving the way for the regeneration of blood vessels. Most previous studies on vascularization in tissue engineering mainly focused on the combination and release patterns of different growth factors, neglecting the structure of the scaffold. In our study, we fabricated the BSF scaffold to combine the sequential release of VEGF and PDGF-BB with a bilayer structure in order to promote the vascularization and regeneration of the bladder.

Effect of BSF scaffold on endothelial differentiation of ADSCs

The endothelial lineage induction of stem cells seeded on scaffolds is also a potential approach to promote vascularization [51]. As a kind of pluripotent stem cell, ADSCs have been confirmed by many studies to possess the ability to differentiate into

endothelial cells [52]. Thus, it is very interesting to explore whether the sequentially released growth factors have a synergistic effect on the endothelial differentiation of ADSCs. Q-PCR analysis showed the highest expression of endothelial marker PECAM-1 and KDR on day 14 (Figure 4A and B). Moreover, both PECAM-1 and KDR had significantly higher expression in the BSF-MS-V/P group than the other groups, indicating that sequential release of VEGF and PDGF-BB promoted the endothelial differentiation of ADSCs better than VEGF or PDGF-BB alone.

The immunofluorescence staining of CD31 and vWF, as well as the uptake capacity of Ac-LDL/UEA-1 were performed to analyze the differentiation of ADSCs toward the endothelial lineage. After 14 days of endothelial induction, the BSF-MS-V/P group showed more cells positive for CD31 staining compared with the BSF-MS, BSF-MS-VEGF and BSF-MS-PDGF groups (Figure 4C and F). Simultaneously, the BSF-MS-V/P group showed more cells positive for vWF staining compared with the BSF-MS, BSF-MS-VEGF and BSF-MS-PDGF groups (Figure 4D and G). Moreover, the BSF-MS-V/P group showed more cells positive for Ac-LDL/UEA-1 double staining compared with the BSF-MS, BSF-MS-VEGF and BSF-MS-PDGF groups, demonstrating the endothelial lineage capacity to uptake Ac-LDL/UEA-1 (Figure 4E and H). Again, these results reveal that the sequential release of VEGF and PDGF-BB has a synergistic effect on the endothelial differentiation of ADSCs. By changing the types of seed cells, angiogenic scaffolds with many other functions can be easily constructed.

Morphological and histological evaluation of BSF patch on rat bladder reconstruction

A variety of congenital and acquired bladder diseases would lead to bladder defects [53–55]. The emergence of bladder tissue engineering brings hope to these patients. Gross photographs of the bladder post-operation showed that the BSF patch could be sutured on the bladder without urine leakage (Figure 5A and B), demonstrating its toughness and waterproofness. Cystography presented that there was no urine leakage in all the groups 4 weeks post-operation. The BSF-MS-V/P group exhibited a larger bladder size compared to the other groups (Figure 5C), indicating its superior reparative effect. Outline of the bladder was smooth in the BSF-MS-V/P group, while it was rough in the other three groups (Figure 5C). As smoother bladder wall means better bladder regeneration, we supposed that the sequential release of VEGF/PDGF-BB and ADSCs made a joint effort to facilitate the regeneration of the reconstructed bladder.

HE staining showed that the BSF patch was partially degraded after 4 weeks (Figure 6A). Except for the BSF-MS group, hyperplasia of urothelial cells was found in the other three groups, indicating regeneration of the urothelium (Figure 6B). Similarly, smooth muscle was seen in all the groups, however the arrangement of smooth muscle fibers seemed to be more disordered in the BSF-MS group (Figure 6C). Masson trichrome staining revealed that there was more collagen deposition in the BSF-MS group than the other three groups (Figure 6D). Notably, more

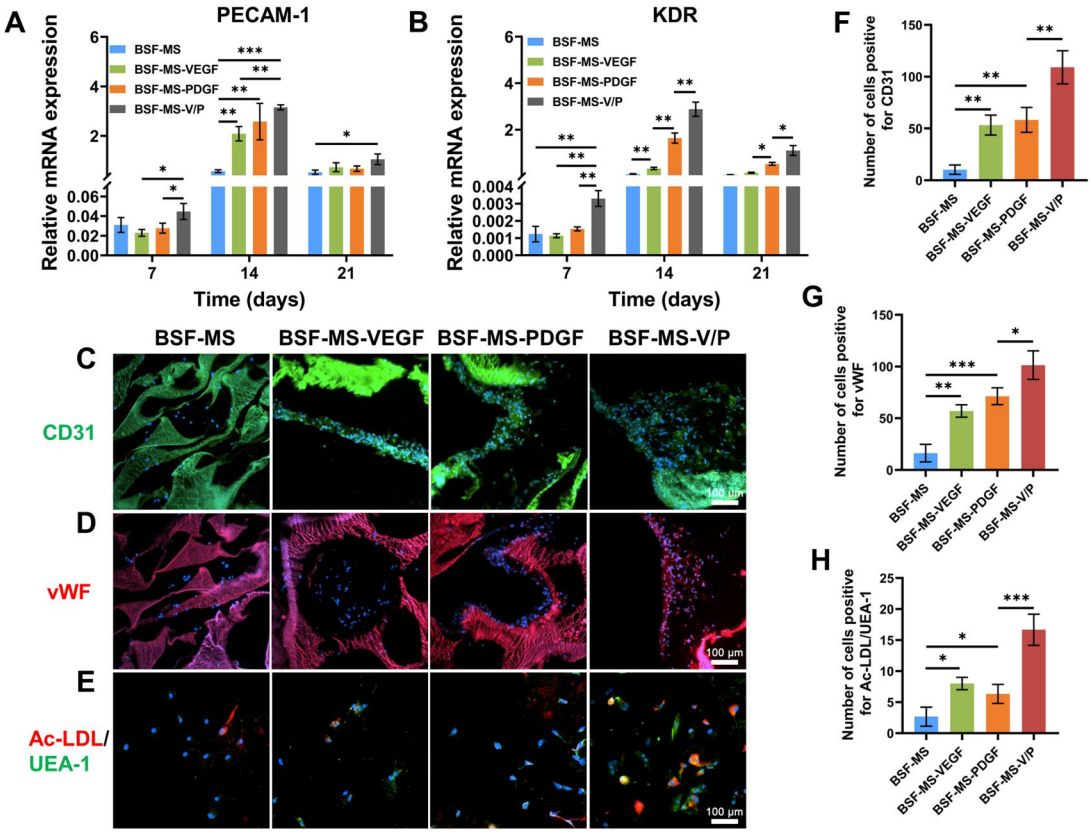

Figure 4. Effect of BSF scaffold on endothelial differentiation of ADSCs. (**A**) Q-PCR analysis of PECAM-1 gene expression on day 7, 14 and 21 ($n = 3$). PECAM-1 gene expression in HUVECs was set as 1. (**B**) Q-PCR analysis of KDR gene expression on day 7, 14 and 21 ($n = 3$). KDR gene expression in HUVECs was set as 1. (**C**) Immunofluorescence staining of CD31 on day 14. (**D**) Immunofluorescence staining of vWF on day 14. (**E**) Uptake of Ac-LDL and UEA-1 on day 14. (**F**) Number of cells positive for CD31 ($n = 3$). (**G**) Number of cells positive for vWF ($n = 3$). (**H**) Number of cells positive for Ac-LDL/UEA-1 double staining ($n = 3$).

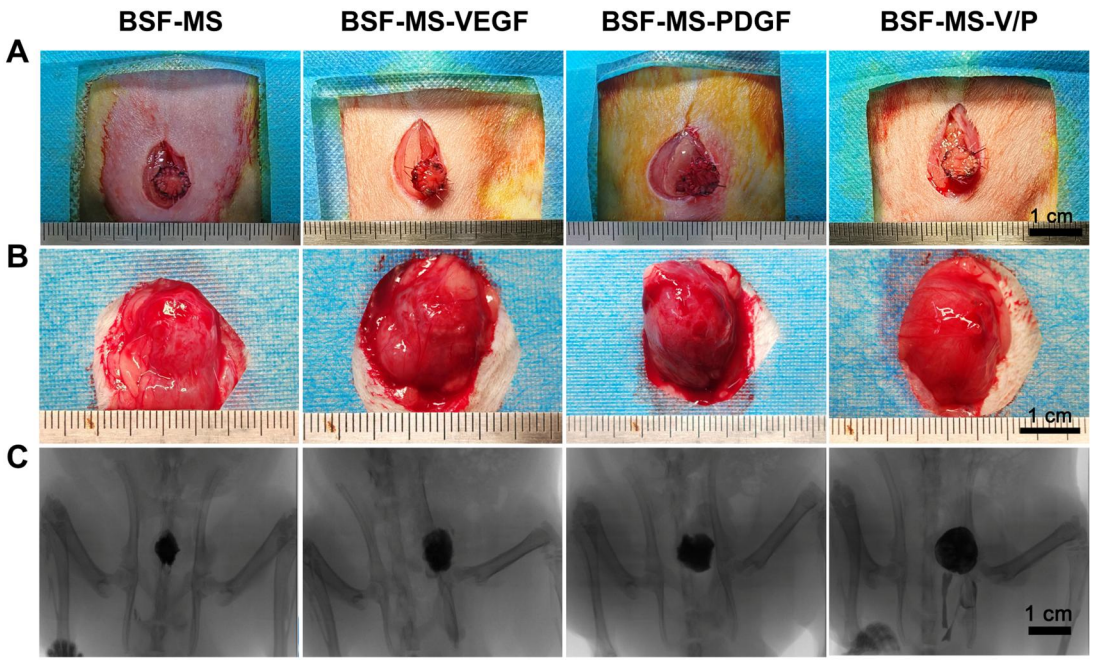

Figure 5. Gross photographs and cystography of BSF patch for rat bladder reconstruction. (**A**) Gross photographs of BSF patch right after the operation. (**B**) Gross photographs of BSF patch 4 weeks post-operation. (**C**) Cystography of the bladder 4 weeks post-operation.

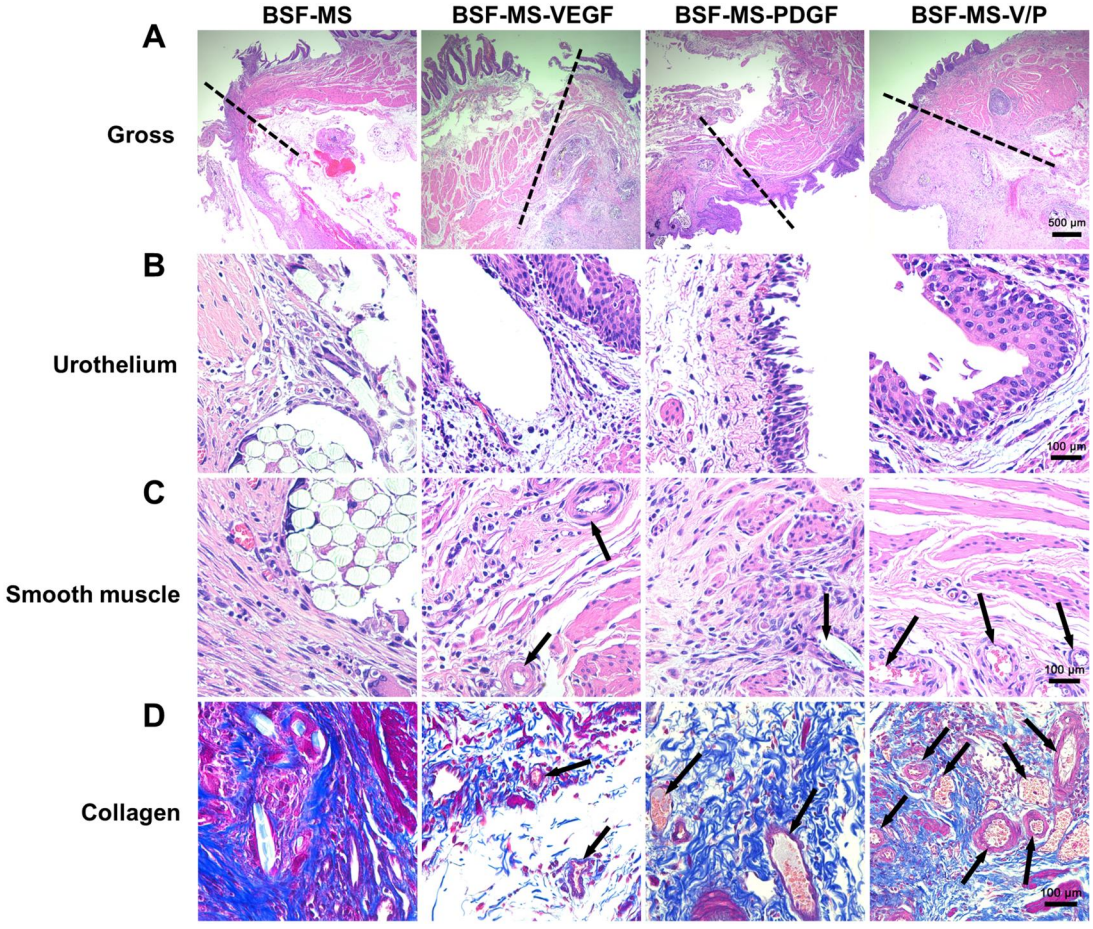

Figure 6. Histological evaluation of BSF patch on rat bladder reconstruction. (**A**) Gross photographs (HE staining) of bladder tissue in the junctional zone. The dotted lines indicate edges of the repaired areas. (**B**) HE staining of the urothelium. (**C**) HE staining of the smooth muscle. The arrows indicate blood vessels. (**D**) Masson trichrome staining of the collagen. The arrows indicate blood vessels.

blood vessels were witnessed in the BSF-MS-V/P group (Figure 6C and D), which was in consistent with previous *in vitro* findings.

Immunofluorescence analyses of BSF patch on vascularization of the reconstructed bladder

Immunofluorescence staining of AE1+AE3, α-SMA and CD31 confirmed the regeneration of urothelium, smooth muscle and endothelium, respectively in all the groups (Figure 7A and B). Blood vessels were demonstrated by double positive staining of α-SMA and CD31 (Figure 7B). Quantitative analyses showed that the blood vessel density and the arteriole density in the BSF-MS-V/P group was significantly higher than the other three groups (Figure 7C and D). Furthermore, the lumen area of blood vessels was significantly larger in the BSF-MS-V/P group (Figure 7E). The distribution and structure of blood vessels were revealed by CD31 and α-SMA double staining. Images of the double staining showed that the blood vessels in the BSF-MS-V/P group was predominantly composed of arteries with abundant smooth muscle, whereas blood vessels in the other three groups were primarily veins with little smooth muscle. These results demonstrated that the sequential release of VEGF and PDGF-BB by the BSF patch promoted vascularization of the reconstructed bladder *in vivo*.

While our experiments exhibited the potential of the BSF patch to enhance vascularization of the tissue-engineered bladder through *in vitro* and *in vivo* analyses, several shortcomings persisted. Firstly, the observation period of 4 weeks post-operation is slightly shorter, long-term follow-ups is encouraged. Moreover, assessing vascularization in larger or thicker scaffolds using large animal models are warranted. In addition, the transformation of ADSCs and their synergistic effect with the sequential release of VEGF and PDGF-BB *in vivo* need in-depth exploration.

Conclusion

We presented a bilayer bioengineered patch with sequential dual-growth factor release to promote vascularization in bladder reconstruction. The outer layer of the scaffold was composed of compact SF film with waterproofness to mimic the serosa of the bladder. The inner layer was constructed of porous SF matrix incorporated with SF microspheres loaded with VEGF and PDGF-BB. The sequential release of these two growth factors was achieved by manipulating the particle size of SF microspheres. *In vitro* studies showed that the BSF scaffold could promote HUVECs migration, tube formation and endothelial differentiation of ADSCs. *In vivo* studies demonstrated that the BSF patch facilitate the regeneration of urothelium, smooth muscle and blood vessels of the reconstructed bladder. In conclusion, our study provided a promising bioengineered patch with vascularization capability for future clinical research.

Funding

This work was financially supported by the National Natural Science Foundation of China (82270721, 81873600).

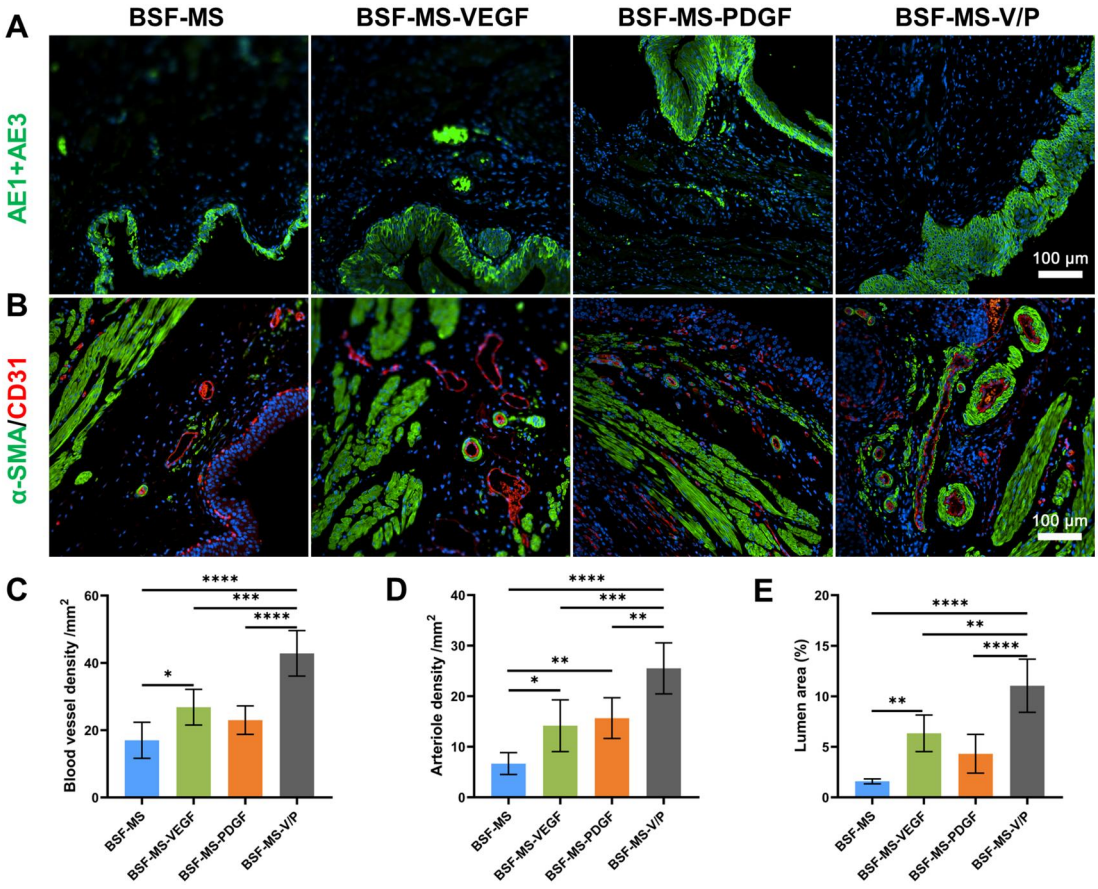

Figure 7. Immunofluorescence analyses of BSF patch on vascularization of the reconstructed bladder. (**A**) AE1+AE3 staining of the urothelium. (**B**) α-SMA and CD31 staining of the smooth muscle and blood vessels. (**C**) Quantification of the blood vessel density ($n = 6$). (**D**) Quantification of the arteriole density ($n = 6$). (**E**) Quantification of the lumen area of blood vessels ($n = 6$).

Supplementary data

Supplementary data are available at *Regenerative Biomaterials* online.

Conflicts of interest statement. None declared.

References

1. Lindskrog SV, Prip F, Lamy P, Taber A, Groeneveld CS, Birkenkamp-Demtröder K, Jensen JB, Strandgaard T, Nordentoft I, Christensen E *et al.* An integrated multi-omics analysis identifies prognostic molecular subtypes of non-muscle-invasive bladder cancer. *Nat Commun* **2021**;12:2301.
2. Casarin M, Morlacco A, Dal Moro F. Tissue engineering and regenerative medicine in pediatric urology: urethral and urinary bladder reconstruction. *Int J Mol Sci* **2022**;23:6360.
3. Cheng PJ, Myers JB. Augmentation cystoplasty in the patient with neurogenic bladder. *World J Urol* **2020**;38:3035–46.
4. Taghavi K, O'Hagan LA, Bortagaray J, Bouty A, Hutson J, O'Brien M. Complication profile of augmentation cystoplasty in contemporary paediatric urology: a 20-year review. *ANZ J Surg* **2021**;91:1005–10.
5. Ying X, Liao L. Augmentation uretero-enterocystoplasty for refractory urinary tract dysfunction: a long-term retrospective study. *BMC Urol* **2021**;21:166.
6. Zhang F, Liao L. Long-term follow-up of neurogenic bladder patients after bladder augmentation with small intestinal submucosa. *World J Urol* **2020**;38:2279–88.
7. Song Y, Li Y, Tian M, Hu J, Zhang X, Liu P, Zhang X, Zhang Q, Zhou L, Zhao L, Li-Ling J, Xie H. Application of antibody-conjugated small intestine submucosa to capture urine-derived stem cells for bladder repair in a rabbit model. *Bioact Mater* **2022**;14:443–55.
8. Sharma S, Basu B. Biomaterials assisted reconstructive urology: the pursuit of an implantable bioengineered neo-urinary bladder. *Biomaterials* **2022**;281:121331.
9. Zhao P, Li X, Fang Q, Wang F, Ao Q, Wang X, Tian X, Tong H, Bai S, Fan J. Surface modification of small intestine submucosa in tissue engineering. *Regen Biomater* **2020**;7:339–48.
10. Zhang X, Jiang Y, Hu J, Zhao L, Chen Q, Liang Y, Zhang Y, Lei X, Wang R, Lei Y, Zhang Q, Li-Ling J, Xie H. Procyanidins-cross-linked small intestine submucosa: a bladder patch promotes smooth muscle regeneration and bladder function restoration in a rabbit model. *Bioact Mater* **2021**;6:1827–38.
11. Atala A. Bladder tissue engineering: the past and the future. *Urology* **2020**;145:337–8.
12. Xiao S, Wang P, Zhao J, Ling Z, An Z, Fu Z, Fu W, Zhou J, Zhang X. Bladder acellular matrix prepared by a self-designed perfusion system and adipose-derived stem cells to promote bladder tissue regeneration. *Front Bioeng Biotechnol* **2022**;10:794603.
13. Sharma S, Mandhani A, Bose S, Basu B. Dynamically crosslinked polydimethylsiloxane-based polyurethanes with contact-killing antimicrobial properties as implantable alloplasts for urological reconstruction. *Acta Biomater* **2021**;129:122–37.
14. Rockwood DN, Preda RC, Yücel T, Wang X, Lovett ML, Kaplan DL. Materials fabrication from bombyx mori silk fibroin. *Nat Protoc* **2011**;6:1612–31.
15. Khademolqorani S, Tavanai H, Chronakis IS, Boisen A, Ajalloueian F. The determinant role of fabrication technique in final characteristics of scaffolds for tissue engineering applications: a focus on silk fibroin-based scaffolds. *Mater Sci Eng C Mater Biol Appl* **2021**;122:111867.
16. Novosel EC, Kleinhans C, Kluger PJ. Vascularization is the key challenge in tissue engineering. *Adv Drug Deliv Rev* **2011**;63:300–11.
17. Rouwkema J, Khademhosseini A. Vascularization and angiogenesis in tissue engineering: beyond creating static networks. *Trends Biotechnol* **2016**;34:733–45.
18. Xiao S, Wang P, Zhao J, Ling Z, An Z, Fu Z, Fu W, Zhang X. Bilayer silk fibroin skeleton and bladder acellular matrix hydrogel encapsulating adipose-derived stem cells for bladder reconstruction. *Biomater Sci* **2021**;9:6169–82.
19. Kant RJ, Coulombe KLK. Integrated approaches to spatiotemporally directing angiogenesis in host and engineered tissues. *Acta Biomater* **2018**;69:42–62.
20. Madub K, Goonoo N, Gimié F, Ait Arsa I, Schönherr H, Bhaw-Luximon A. Green seaweeds ulvan-cellulose scaffolds enhance in vitro cell growth and in vivo angiogenesis for skin tissue engineering. *Carbohydr Polym* **2021**;251:117025.
21. Wang X, Lin M, Kang Y. Engineering porous β-tricalcium phosphate (β-TCP) scaffolds with multiple channels to promote cell migration, proliferation, and angiogenesis. *ACS Appl Mater Interfaces* **2019**;11:9223–32.
22. Hsu Y, Wei S, Lin T, Fang L, Hsieh Y, Chen Y. A strategy to engineer vascularized tissue constructs by optimizing and maintaining the geometry. *Acta Biomater* **2022**;138:254–72.
23. Eichholz KF, Freeman FE, Pitacco P, Nulty J, Ahern D, Burdis R, Browe DC, Garcia O, Hoey DA, Kelly DJ. Scaffold microarchitecture regulates angiogenesis and the regeneration of large bone defects. *Biofabrication* **2022**;14:045013.
24. Wu Y, Song L, Shafiq M, Ijima H, Kim SH, Wei R, Kong D, Mo X, Wang K. Peptides-tethered vascular grafts enable blood vessel regeneration via endogenous cell recruitment and neovascularization. *Compos B: Eng* **2023**;252:110504.
25. Ding T, Kang W, Li J, Yu L, Ge S. An in situ tissue engineering scaffold with growth factors combining angiogenesis and osteoimmunomodulatory functions for advanced periodontal bone regeneration. *J Nanobiotechnol* **2021**;19:247.
26. Ahmad A, Nawaz MI. Molecular mechanism of VEGF and its role in pathological angiogenesis. *J Cell Biochem* **2022**;123:1938–65.
27. Zhao F, Xu S, Zhang C, Liu J, Zhang Y, Yang J, Xing X. PDGF mediates pulmonary arterial smooth muscle cell proliferation and migration by regulating NFATc2. *Mol Med Rep* **2021**;23:39.
28. O'Brien EM, Risser GE, Spiller KL. Sequential drug delivery to modulate macrophage behavior and enhance implant integration. *Adv Drug Deliv Rev* **2019**;149–150:85–94.
29. Wang X, Yucel T, Lu Q, Hu X, Kaplan DL. Silk nanospheres and microspheres from silk/PVA blend films for drug delivery. *Biomaterials* **2010**;31:1025–35.
30. Wei J, Xia X, Xiao S, Zou JS, Zuo Q, Li Y, Li J. Sequential dual-biofactor release from the scaffold of mesoporous HA microspheres and PLGA matrix for boosting endogenous bone regeneration. *Adv Healthc Mater* **2023**;12:e2300624.
31. Moreno-Manzano V, Mellado-López M, Morera-Esteve MJ, Alastrue-Agudo A, Bisbal-Velasco V, Forteza-Vila J, Serrano-Aroca Á, Vera-Donoso CD. Human adipose-derived mesenchymal stem cells accelerate decellularized neobladder regeneration. *Regen Biomater* **2020**;7:161–9.
32. Yang T, Zhao F, Zhou L, Liu J, Xu L, Dou Q, Xu Z, Jia R. Therapeutic potential of adipose-derived mesenchymal stem cell exosomes in tissue-engineered bladders. *J Tissue Eng* **2021**;12:20417314211001545.
33. Moreno-Manzano V, Zaytseva-Zotova D, López-Mocholí E, Briz-Redón Á, Løkensgard Strand B, Serrano-Aroca Á. Injectable gel

form of a decellularized bladder induces adipose-derived stem cell differentiation into smooth muscle cells in vitro. *Int J Mol Sci* **2020**;21:8608.
34. Suresh V, West JL. 3D culture facilitates VEGF-stimulated endothelial differentiation of adipose-derived stem cells. *Ann Biomed Eng* **2020**;48:1034–44.
35. Shrestha KR, Jeon SH, Jung AR, Kim IG, Kim GE, Park YH, Kim SH, Lee JY. Stem cells seeded on multilayered scaffolds implanted into an injured bladder rat model improves bladder function. *Tissue Eng Regen Med* **2019**;16:201–12.
36. Zhang W, Ling C, Zhang A, Liu H, Jiang Y, Li X, Sheng R, Yao Q, Chen J. An all-silk-derived functional nanosphere matrix for sequential biomolecule delivery and in situ osteochondral regeneration. *Bioact Mater* **2020**;5:832–43.
37. Xia H, Wang L, Li C, Tian B, Li Q, Zhao H, Bai Q. Synthesis of fully porous silica microspheres with high specific surface area for fast HPLC separation of intact proteins and digests of ovalbumin. *Mikrochim Acta* **2020**;187:382.
38. Yang X, Tian Z, Guo K, Lu T, Ji J, Hao S, Xiao S. Preparation and mechanism of hydroxyapatite hollow microspheres with different surface charge by biomimetic method. *J Mater Sci Mater Med* **2020**;31:47.
39. Nahum V, Domb AJ. Solid lipid microspheres decorated nanoparticles as drug carriers. *Int J Pharm* **2022**;621:121797.
40. Yang F, Xu C, Zhang W, Sun L, Feng G, Ning T, Wang W, Sun B, Li J, Niu X, Fan Y. Biodegradable magnesium incorporated microspheres enable immunomodulation and spatiotemporal drug release for the treatment of osteonecrosis of the femoral head. *Compos B: Eng* **2023**;250:110430.
41. Wu B, Wu L, He Y, Yin Z, Deng L. Engineered PLGA microspheres for extended release of brexpiprazole: in vitro and in vivo studies. *Drug Dev Ind Pharm* **2021**;47:1001–10.
42. Subbiah R, Guldberg RE. Materials science and design principles of growth factor delivery systems in tissue engineering and regenerative medicine. *Adv Healthc Mater* **2019**;8:e1801000.
43. Goins A, Webb AR, Allen JB. Multi-layer approaches to scaffold-based small diameter vessel engineering: a review. *Mater Sci Eng C Mater Biol Appl* **2019**;97:896–912.
44. Kamrani A, Nasrabadi MH, Halabian R, Ghorbani M. A biomimetic multi-layer scaffold with collagen and zinc doped bioglass as a skin-regeneration agent in full-thickness injuries and its effects in vitro and in vivo. *Int J Biol Macromol* **2023**;253:127163.
45. Li M, Song P, Wang W, Xu Y, Li J, Wu L, Gui X, Zeng Z, Zhou Z, Liu M, Kong Q, Fan Y, Zhang X, Zhou C, Liu L. Preparation and characterization of biomimetic gradient multi-layer cell-laden scaffolds for osteochondral integrated repair. *J Mater Chem B* **2022**;10:4172–88.
46. Carrow JK, Di Luca A, Dolatshahi-Pirouz A, Moroni L, Gaharwar AK. 3D-printed bioactive scaffolds from nanosilicates and PEOT/PBT for bone tissue engineering. *Regen Biomater* **2019**;6:29–37.
47. Chen J, Zhang D, Wu L, Zhao M. Current strategies for engineered vascular grafts and vascularized tissue engineering. *Polymers (Basel)* **2023**;15:2015.
48. Akbarian M, Bertassoni LE, Tayebi L. Biological aspects in controlling angiogenesis: current progress. *Cell Mol Life Sci* **2022**;79:349.
49. Jiang X, Xiong Q, Xu G, Lin H, Fang X, Cui D, Xu M, Chen F, Geng H. VEGF-loaded nanoparticle-modified BAMAs enhance angiogenesis and inhibit graft shrinkage in tissue-engineered bladder. *Ann Biomed Eng* **2015**;43:2577–86.
50. Tien J. Tissue engineering of the microvasculature. *Compr Physiol* **2019**;9:1155–212.
51. Sun X, Altalhi W, Nunes SS. Vascularization strategies of engineered tissues and their application in cardiac regeneration. *Adv Drug Deliv Rev* **2016**;96:183–94.
52. Deng M, Gu Y, Liu Z, Qi Y, Ma GE, Kang N. Endothelial differentiation of human adipose-derived stem cells on polyglycolic acid/polylactic acid mesh. *Stem Cells Int* **2015**;2015:350718.
53. Gernone F, Uva A, Cavalera MA, Zatelli A. Neurogenic bladder in dogs, cats and humans: a comparative review of neurological diseases. *Animals (Basel)* **2022**;12:3233.
54. Lenis AT, Lec PM, Chamie K, Mshs MD. Bladder cancer: a review. *JAMA* **2020**;324:1980–91.
55. Reutter H, Holmdahl G. Genetic counseling for bladder exstrophy-epispadias complex. *Eur J Pediatr Surg* **2021**;31:468–71.

Regenerative Biomaterials, 2024, 11, 1–11
https://doi.org/10.1093/rb/rbae083
Research article